IOP Publishing Journal of Physics: Condensed Matter
J. Phys.: Condens. Matter **32** (2020) 224003 (9pp) https://doi.org/10.1088/1361-648X/ab73a6

Effect of copper concentration on the structure and properties of Al–Cu–Fe and Al–Cu–Ni melts

L V Kamaeva[1,2], R E Ryltsev[2,3,4], A A Suslov[1] and N M Chtchelkatchev[2,4,5]

[1] Udmurt Federal Research Center, Ural Branch of Russian Academy of Sciences, 426068 Izhevsk, Russia
[2] Vereshchagin Institute for High Pressure Physics, Russian Academy of Sciences, 108840 Troitsk, Moscow, Russia
[3] Institute of Metallurgy, Ural Branch of Russian Academy of Sciences, 620016, Ekaterinburg, Russia
[4] Ural Federal University, 620002, Ekaterinburg, Russia
[5] Moscow Institute of Physics and Technology, 141700, Dolgoprudny, Moscow Region, Russia

E-mail: lara_kam@mail.ru

Received 11 November 2019, revised 21 January 2020
Accepted for publication 6 February 2020
Published 5 March 2020

Abstract

We address a relationship between properties of liquid and solid states by comparing structural characteristics and viscosity in Al–Cu–Fe and Al–Cu–Ni melts. The former system forms an equilibrium quasicrystalline phase but the latter does not. We show that the concentration behavior of the viscosity, melting temperature and characteristics of the chemical short-range order correlate with each other. The main structural differences between the melts are related to the peculiarities of their electronic structure, which is the same for liquid and solid states near the melting temperature.

Keywords: liquid alloy, viscosity, short-range order, electronic structure

(Some figures may appear in colour only in the online journal)

1. Introduction

The relation between structural properties of liquid metals and the solids formed during their amorphization or crystallization has been intensively discussed [1–5]. For example, in the case of amorphization of metallic alloys, the relationship between structural-sensitive liquid phase properties (viscosity, thermal expansion, etc) and glass-forming ability is often discussed [2, 6–8]. More controversial is the possibility of inheriting structural motifs of the initial melt by the structure of solid phases. Illustrative examples are quasicrystals in metallic alloys, whose formation is often associated with the icosahedral short-range order in the melts. Promising objects to address these issues are Al-based systems, in which complex crystal structures, as well as equilibrium quasicrystalline phases, are observed [9, 10]. In this paper, we focus on two Al-based systems: Al–Cu–Fe and Al–Cu–Ni.

The Al–Cu–Fe is one of the first metallic systems in which the formation of a stable icosahedral phase (i-phase) was reported [11]. The i-phase can be produced by different methods: melt solidification with subsequent annealing, rapid quenching techniques (such as melt spinning), gas atomization and mechanical alloying [12]. As follows from the Al–Cu–Fe phase diagram [13], besides the i-phase, binary AlCu, Al_2Cu, Al_7Fe_2, Al_3Fe ($Al_{13}Fe_4$), Al_5Fe_2, $AlFe_3$, Al_2Cu,Fe_5 phases, β-AlFe(Cu) solid solution, and triple $Al_{10}Cu_{10}Fe$, $Al_{18}Cu_{10}Fe$, Al_7Cu_2Fe phases have been found in the system. The stoichiometry compositions of experimentally fabricated i-phases in Al–Cu–Fe vary from 25 at.% Cu and 10 at.% Fe to 28.6 at.% Cu and 13.8 at.% Cu depending on the production method. Within the compositional range of 30–40 at.% Cu, the i-phase can be formed by peritectic reactions, and, at 2–6 at.% Fe, it can be directly formed from the melt. However, in the latter case, i-phase is non-equilibrium at room temperature.

The Al–Cu–Ni system does not form quasicrystal phases, but 12 different solid phases are found [14]. These are 9 binary phases in the Al-rich region, such as Al_3Ni, Al_3Ni_2, Al_4Ni_3, Al_2Cu, two solid solutions (the first one is Al-based with Ni dissolved and the second one is Ni–Cu-based with Al dissolved) and one triple τ—phase $(Ni, Cu)_3Al_5$.

Thus, in the Al-rich region, the systems under consideration have similar phase diagrams; their main difference is the existence of i-phase in the Al–Cu–Fe system. To address the relationship between the structure of liquid and solid states, it is interesting to compare the features of interatomic interaction in the melts of these systems. Therefore, in this work, we study the structural characteristics and viscosity of Al–Cu–Fe and Al–Cu–Ni melts in the region of aluminum and copper concentrations corresponding to the stoichiometry of the i-phase in the former system: $Al_{100-x}Cu_xFe_{12.5}$, where $x = 15.5$–35.5 and $Al_{100-x}Cu_xNi_{10}$, where $x = 17.5$–40. Note that, for the Al–Cu–Ni system, we choose concentration cross-section in which it demonstrates similar phase transformations as for the Al–Cu–Fe one.

Viscosity is one of the main structural-sensitive properties of a fluid. For metal melts, it is also of practical importance because the viscosity value affects significantly the casting process. Moreover, the analysis of the viscosity allows estimating qualitatively how the interatomic interaction in a melt varies with a change of atomic concentration [15, 16].

The concentration behavior of the viscosity in binary Al–Cu, Al–Ni, and Al–Fe systems has been intensively studied by experimental and theoretical methods [17–25]. The results on viscosity obtained by different authors are somewhat different, but most researchers find a pronounced nonlinear dependence of viscosity on composition in these systems. In [23, 24], molecular dynamics (MD) simulations revealed that such behavior of the viscosity is caused by concentration changes in local structural ordering (icosahedral short-range order and chemical short-range order). According to [23, 24], such structural evolution in Al–Ni and Al–Cu melts at high Ni and Cu concentrations can lead to a violation of the Stokes–Einstein relation.

The viscosity of ternary Al–Cu–(Fe, Ni) systems is much less studied. In [26], the temperature dependence of the viscosity of the $Al_{63}Cu_{25}Fe_{12}$ melt was studied. The authors revealed a kink at 1473 K on the viscosity polytherms and explained it by the destruction of icosahedral short-range order. However, later we showed that this feature does not reflex any structural changes but rather associated with methodological shortcomings in measuring the viscosity by the torsional vibrations method [27]. As far as we know, there is no available data on the viscosity of Al–Cu–Ni melts.

The lack of reliable information on the viscosity of Al–Cu–(Fe,Ni) melts is primarily due to the complexity of the high-temperature viscometric experiment. However, earlier we developed a precision technique, which takes into account the effect of surface oxide layers and allows obtaining reliable data on the viscosity of metallic melts [16, 25, 27, 28].

Thus the main purpose of the paper is to address a relationship between properties of liquid and solid states in Al–Cu–(Fe,Ni) melts by comparing their structural characteristics and viscosity.

2. Methods

The systems studied were fabricated by alloying the corresponding proportions of Al–Ni, Cu–Ni, Al–Fe master alloys ($Al_{90}Ni_{10}$, $Cu_{90}Ni_{10}$ and $Al_{80.6}Fe_{19.4}$ or $Al_{69.8}Fe_{30.2}$ depending on the melted composition), electrolytic aluminum (A999-type), and cathode copper, in a viscosimeter furnace in an inert atmosphere of He (after preliminary pumping to 10^{-2} Pa) at $T = 1773$ K for 1 h. The synthesis of ligatures was carried out according to the traditional metallurgical technology by alloying electrolytic Al and cathode Cu, Ni and Fe in a vacuum furnace at $T = 1773$ K for 30 min. The chemical composition of the obtained samples was determined by atomic emission spectroscopy on a Spectroflame spectrometer (for both the main components and impurities).

Kinematic viscosity ν was measured by the method of damped torsional vibrations of a corundum crucible with a melt [29]. The experiments were carried out in an atmosphere of purified helium by using crucibles of aluminum oxide. To prevent an uncontrollable influence of the oxide surface film, a cover of Al_2O_3 was placed on the melt surface and fixed so that it served as a second end surface of the crucible [30]. Preliminary experiments for Al–Cu–Fe melts have shown that, immediately after melting, the alloys under consideration demonstrate slow relaxation of the viscosity (2 h or more). The reason is the slow establishment of thermodynamic equilibrium in the melt-crucible-atmosphere system [27]. This feature must be taken into account when measuring the temperature dependencies of viscosity $\nu(T)$. Therefore, measurements of $\nu(T)$ were performed in the following mode. After melting, a liquid was overheated by 50 K above the liquidus temperature, kept at this temperature for 10 minutes and then cooled to the liquidus temperature. Then, we performed viscosity measurements by heating a system in a stepwise manner from the melting temperature up to 1773 K by increments of 20–30 K and then cooling it down to melting temperature; at each temperature, isothermal exposure of 7 min was performed before measurement. Next, the samples were cooled down to room temperature and the above stages were cyclically repeated. The melting points of the alloys were determined by using a high-temperature thermal analyzer [31].

For all investigated melts, in whole temperature ranges, temperature dependencies $\nu(T)$ obtained in both heating and cooling modes, are well fitted by the Arrhenius relation:

$$\nu = A_\nu e^{\frac{E_\nu}{RT}}, \quad (1)$$

where A_ν is the pre-exponential factor; E_ν is the activation energy; R is the universal gas constant; T is the absolute temperature.

To construct concentration dependencies of the viscosity for each alloy, we fit the viscosity data obtained in two subsequent

Table 1. Parameters of equation (1) for temperature dependencies ν of Al–Cu–Ni melts.

Composition	A_v, 10^{-8} m^2 s^{-1}	E_v, kJ mol^{-1}	Composition	A_v, 10^{-8} m^2 s^{-1}	E_v, kJ mol^{-1}
$Al_{72.5}Cu_{17.5}Ni_{10}$	11.3	19.1	$Al_{60}Cu_{30}Ni_{10}$	7.7	25.4
$Al_{70}Cu_{20}Ni_{10}$	9.6	20.8	$Al_{57.5}Cu_{32.5}Ni_{10}$	8.7	23.9
$Al_{69}Cu_{21}Ni_{10}$	8.8	17.7	$Al_{55}Cu_{35}Ni_{10}$	7.2	26.3
$Al_{67.5}Cu_{22.5}Ni_{10}$	8.7	20.5	$Al_{54}Cu_{36}Ni_{10}$	5.8	28.2
$Al_{66}Cu_{24}Ni_{10}$	8.2	22.3	$Al_{52.5}Cu_{37.5}Ni_{10}$	6.8	27.5
$Al_{65}Cu_{25}Ni_{10}$	6.5	26.1	$Al_{51}Cu_{39}Ni_{10}$	7.7	25.7
$Al_{62.5}Cu_{27.5}Ni_{10}$	10.5	20.8	$Al_{50}Cu_{40}Ni_{10}$	8.2	26.1

heating/cooling cycles by common exponential dependence. For the Al–Cu–Fe melts, data on the temperature dependences of viscosity are taken from [27]; the corresponding parameters of the equation (1) for the studied Al–Cu–Ni alloys are presented in table 1.

For a confidence probability of 0.95, the most probable error in determining the absolute values of the viscosity of Al–Cu–Fe melts in a single experiment is 2.5% with a total error of no more than 5%.

The structural characteristics of the melts were determined by using *ab initio* molecular dynamics (AIMD) simulations. The calculations were performed by using the Vienna *ab initio* simulation program [32]. Projector augmented-wave pseudopotentials and Perdew–Burke–Ernzerhof [33, 34] gradient approximation to the exchange-correlation functional were used [35]. The wave function was expanded by the plane-wave basis set in the periodic boundary condition, and plane wave cut-off energy was 500 eV. Only Γ-point was used for sampling the Brillouin zone [9].

Cubic supercells of 512 atoms with the following compositions were built: $Al_{69.5}$ $Cu_{18}Fe_{12.5}$, $Al_{62}Cu_{25.5}Fe_{12.5}$, $Al_{52}Cu_{35.5}Fe_{12.5}$, $Al_{72.5}$ $Cu_{17.5}$ Ni_{10}, $Al_{67.5}$ $Cu_{22.5}$ Ni_{10}, Al_{65} Cu_{25} Ni_{10}, Al_{60} Cu_{30} Ni_{10}, $Al_{52.5}$ $Cu_{37.5}$ Ni_{10}, and $Al_{50}Cu_{40}Ni_{10}$. To prepare the initial liquid configuration for one of the compositions we melted the crystal of randomly distributed 512 atoms and annealed the melt at 3000 K and zero pressure $P = 0$ for at least 20 ps. For all the other alloy compositions we used different much faster procedure described below.

To prepare initial configuration for a liquid alloy with a target composition, we took a configuration from a previous simulation run (at 3000 K and $P = 0$) corresponding to some initial composition, then changed the alloy composition in the input configuration file and run the search of quasirandom configuration using USPEX genetic evolutionary algorithm [36–38] to prepare the 'most disordered' alloy structure. Such a calculation usually takes about 24 h and required only one processor core. It should be noted that this procedure does not perform AIMD but permutes atoms quasirandomly (accepting swaps that increase entropy) and simultaneously most evenly and randomly distributes the alloy components throughout the available cell taking into account periodicity and avoiding clustering as much as possible [39]. Note that this procedure is different from a simple random permutation of atoms by a random number generator. Thanks to this algorithm, we do not have to spend much supercomputer time melting the crystal with a target composition and equilibrating the melt (we have to do it one time for a first composition). It also allows us to reduce significantly the relaxation time. Then, for each configuration, prepared this way, we perform AIMD equilibration enabling the system to evolve from quasirandom configurations to 'true' ones corresponding to target temperature. Such equilibration was performed in several steps. First, we performed initial NPT equilibration at $P = 0$ and $T = 3000$ K to relax equilibrium volume simulations and then switching to NVT ensemble (it allows a much faster AIMD simulation) we annealed the system during 10 ps. Using elevated temperature allows for equilibrating the system faster. After that, we cooled the configuration in NPT ensemble to the target temperature (slightly above the experimental melting temperature) at $P = 0$ and equilibrated it to obtain equilibrium density (MD cell volume). At the final step, we run NVT simulations for calculating correlation functions and observable properties.

Calculations of the radial distribution functions (RDFs) were performed using the results of AIMD simulation in the NVT ensemble at the density corresponding to zero pressure $P = 0$ using visual molecular dynamics (VMD) software [40]. The length of AIMD trajectory was 10–20 ps (5–10 thousand MD steps with the time step of 2 fs).

To verify AIMD calculations, we compare experimental and calculated structure factors of the melts under consideration. First, we perform an x-ray diffraction study of Al–Cu–Fe and Al–Cu–Ni melt structures. The x-ray diffraction was carried out on a diffractometer with a high-temperature chamber. The Bragg–Brentano law was used for focussing with Mo-Kα radiation; Kβ reflection was suppressed using a graphite monochromator. X-ray diffraction patterns were obtained with two-second exposure and 0.1 angle step increments. An open-surface sample was placed in an Al_2O_3 crucible horizontally. The necessary spatial position is provided by the vertical movement of the sample. The measurements were performed under a protective atmosphere of helium. The obtained experimental diffraction patterns were calculated into a structure factor using RAD program [41]. However, due to methodological features, high-quality x-ray diffraction patterns were obtained only for Al–Cu–Fe samples from the region where the i-phase does not exist, for example, the $Al_{58.7}Cu_{35.5}Fe_{5.8}$ alloy. Therefore, we performed AIMD simulations for this alloy and then calculated the structure factor. We see a good agreement between the experimental and calculated structure factors (figure 1). That suggests pair correlation functions extracted from AIMD data RDFs describe accurately the structure of the melts under study.

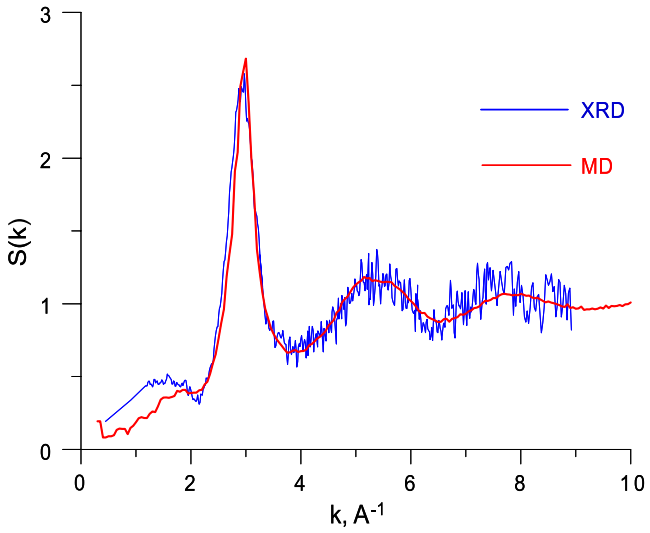

Figure 1. Comparison of the structural factors of $Al_{58.7}Cu_{35.5}Fe_{5.8}$ melt obtained from experimental x-ray scattering data (blue line) and AIMD (red line).

By using RDFs, one can determine useful structural characteristics, such as distance between nearest neighbors r_{i-j} and coordination number Z_{i-j}. The former is determined from the positions of the first peaks of partial RDFs, and the latter is calculated by integrating the partial RDFs to their first minima; the area under the first peak of total RDF is equal to the number of nearest neighbors in the first coordination sphere. To analyze chemical SRO, we calculate Warren–Cowley parameters [9, 42], which are extracted from both total and partial coordination numbers as:

$$\alpha_{i-j} = 1 - \frac{Z_{i-j}}{Z_{i-\text{total}} x_j}. \quad (2)$$

Here $Z_{i-\text{total}}$ and Z_{i-j} are respectively the total and partial coordination numbers, x_j is the j atom concentration. For a random atom distribution, α_{i-j} are equal to zero. The negative/positive value of α_{i-j} means that the average concentration of the element j in the nearest neighborhood of the element i is more/less than for the random distribution. To describe such behaviour we shall hereafter use the terms effective attraction/repulsion between i and j species.

3. Results

The experimentally obtained viscosity isotherms of Al–Cu–Fe and Al–Cu–Ni melts along two concentration cross-sections at $x_{Fe} = 12.5$ at.% and $x_{Ni} = 10$ at.% are shown in figure 2. It can be seen from the figures that the replacement of aluminum by copper has little effect on the viscosity of Al–Cu–Fe melts in the investigated concentration range. On the concentration dependence $\nu(x_{Cu})$ obtained at $x_{Fe} = 12.5$ at.%, we observe weakly pronounced minimum at $x_{Cu} = 25$ at.% (figure 2(a)); at $x_{Cu} > 30$ at.%, viscosity is constant within the range of measurement error (figure 2(a)). The viscosity of the Al–Cu–Ni system is more sensitive to changes in copper concentration. Replacing Al atoms with Cu ones leads to an increase in viscosity, but a clear minimum is observed in the region of 21 at.% Cu. (figure 2(b)).

An increase in temperature leads to a weakening of the concentration dependence of the viscosity. However, general properties of $\nu(x)$ dependence remain the same up to 1673 K (figures 2(a) and (b)). The main features of the viscosity of the Al–Cu–(Fe,Ni) melts along the studied concentration cross-sections are in good agreement with the concentration dependencies on the melting temperature of these alloys (figures 2(c) and (d)). In Al–Cu–Fe alloys, the dependence of the melting temperature (T_m) on the Cu concentration x_{Cu} develops a minimum at $x_{Cu} = 25.5$ at.% Cu (figure 2(c)). According to [13], this minimum corresponds to invariant equilibrium reaction: $L \rightarrow L + Al_3Fe + \beta$, where β is either the B2 structure or corresponding disordered solid solution. For Al–Cu–Ni alloys in the temperature range from 1200 to 1500 K, T_m increases monotonically as the x_{Cu} increases. However, a kink is observed at $x_{Cu} = 21$ at.% (figure 2(d)) which corresponds to the phase transformation $L \rightarrow L + Al_3\,Fe + (\beta,\text{AlNi})$, where β is B2 phase based on AlNi [14].

Since the viscosity is a structural-sensitive property [15, 16, 31], the features of its concentration dependencies may indicate structural changes in the melt. Therefore, taking into account the detected minima of viscosity, the following compositions were selected for AIMD simulations: $Al_{69.5}Cu_{18}Fe_{12.5}$, $Al_{62}Cu_{25.5}Fe_{12.5}$, $Al_{52}Cu_{35.5}Fe_{12.5}$, $Al_{72.5}Cu_{17.5}Ni_{10}$, $Al_{67.5}Cu_{22.5}Ni_{10}$, $Al_{65}Cu_{25}Ni_{10}$, $Al_{60}Cu_{30}Ni_{10}$, $Al_{52.5}Cu_{37.5}Ni_{10}$, and $Al_{50}Cu_{40}Ni_{10}$. Since the melting point of Al–Cu–Fe alloys depends weakly on the Cu concentration (figure 2(c)), these alloys were simulated at temperatures 100 K above corresponding T_m; for Al–Cu–Ni alloys simulations have been performed at the same temperature, 1673 K.

Using AIMD simulations, we calculate the total and partial radial distribution functions (RDFs) $g(r)$ as well as corresponding cumulative RDFs $Z(r)$ reflecting distance-dependent coordination numbers. In figures 3 and 4 we show these functions for the three studied compositions Al–Cu–Fe (figure 3) and six Al–Cu–Ni (figure 4). We see that total RDFs as well as partial Al-total, Cu-total, Al–Al, Al–Cu, and Cu–Cu ones are similar to that for simple liquids like Lennard-Jones one. That means there is no strong chemical interaction between Cu–Cu, Al–Al and Cu–Al in the Al–Cu–Fe and Al–Cu–Ni melts. However, a comparison of partial RDFs shows what interaction between Al and Cu is slightly higher than for Al–Al and Cu–Cu in both systems. Indeed, the ratio $g(r_{max})/g(r_{min})$ for g_{Al-Cu} is visually higher than for g_{Cu-Cu} and g_{Al-Al} (where r_{max} and r_{min} are the positions of the first maximum and the first minimum respectively). The more rigorous analysis will be performed below using the Warren-Cawley parameters (see figure 5).

The shapes of $g_{Fe\text{-total}}(r)$ and $g_{Ni\text{-total}}(r)$ curves reveal much more pronounced RDF peaks, especially at low Cu concentrations. Analysis of partial Fe–Al, Fe–Cu, Fe–Fe and Ni–Al, Ni–Cu, Ni–Ni RDFs clarifies this behaviour. We see that for Al–Cu–Fe system the $g_{Fe-Al}(r)$ demonstrates two features: the low values of the first minimum and very pronounced first peaks, especially for small Cu concentration. At the same

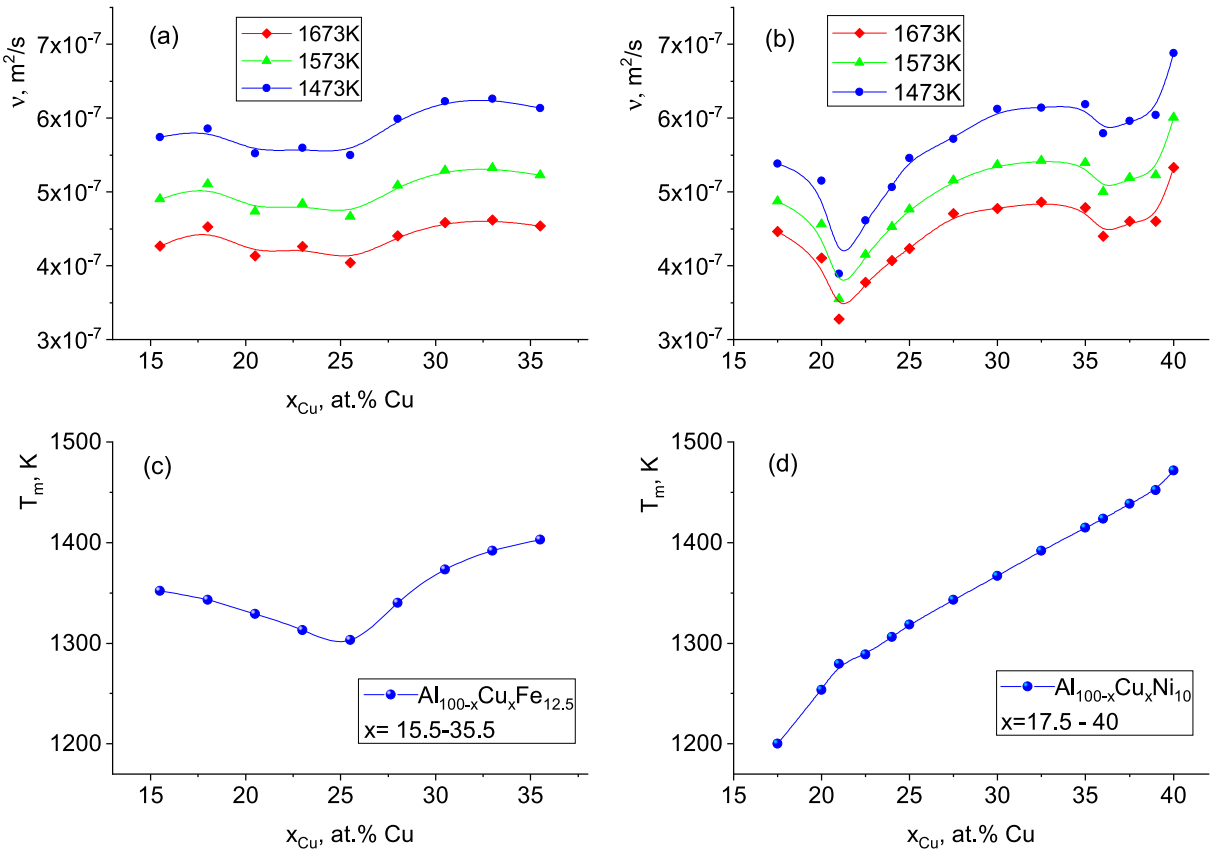

Figure 2. ((a) and (b)) Concentration dependencies of the viscosity of Al–Cu–Fe and Al–Cu–Ni melts at $x_{\mathrm{Fe}} = 12.5$ (a) and $x_{\mathrm{Ni}} = 10$ at.% (b) and different temperatures. ((c) and (d)) Concentration dependencies of melting points T_m.

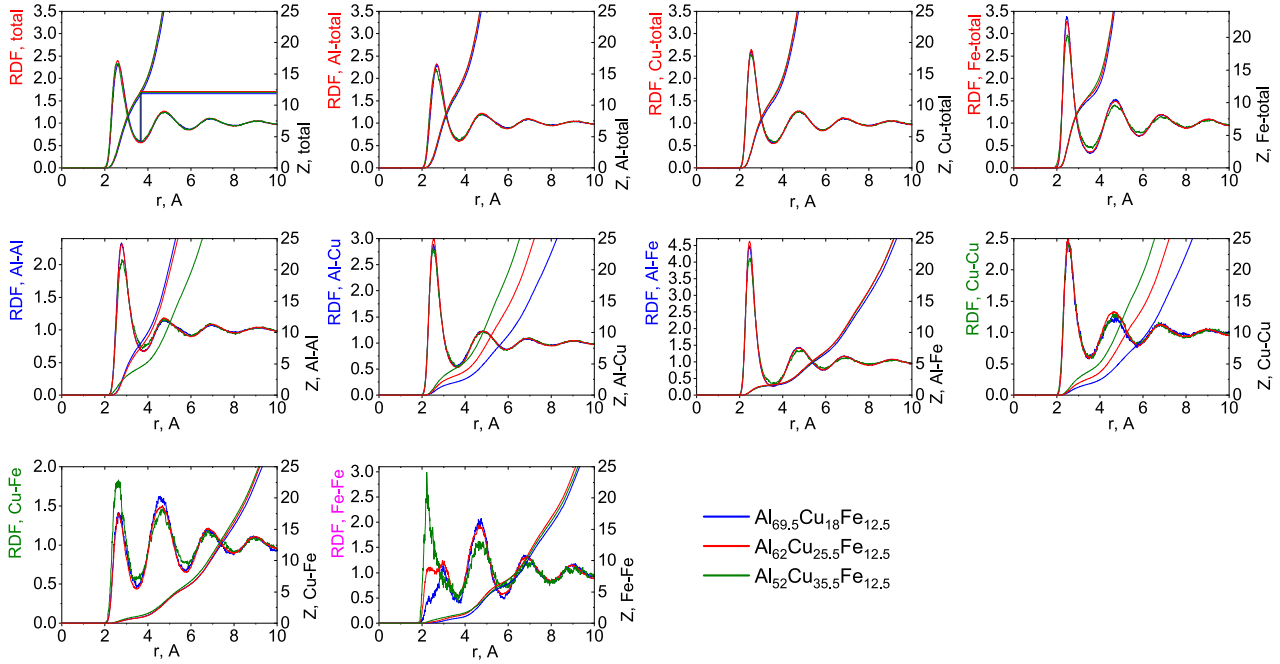

Figure 3. Total and partial RDFs $g(r)$ and coordination numbers $Z(r)$ extracted from *ab initio* molecular dynamics simulations for several Al–Cu–Fe melts at temperatures 100 K above corresponding melting points.

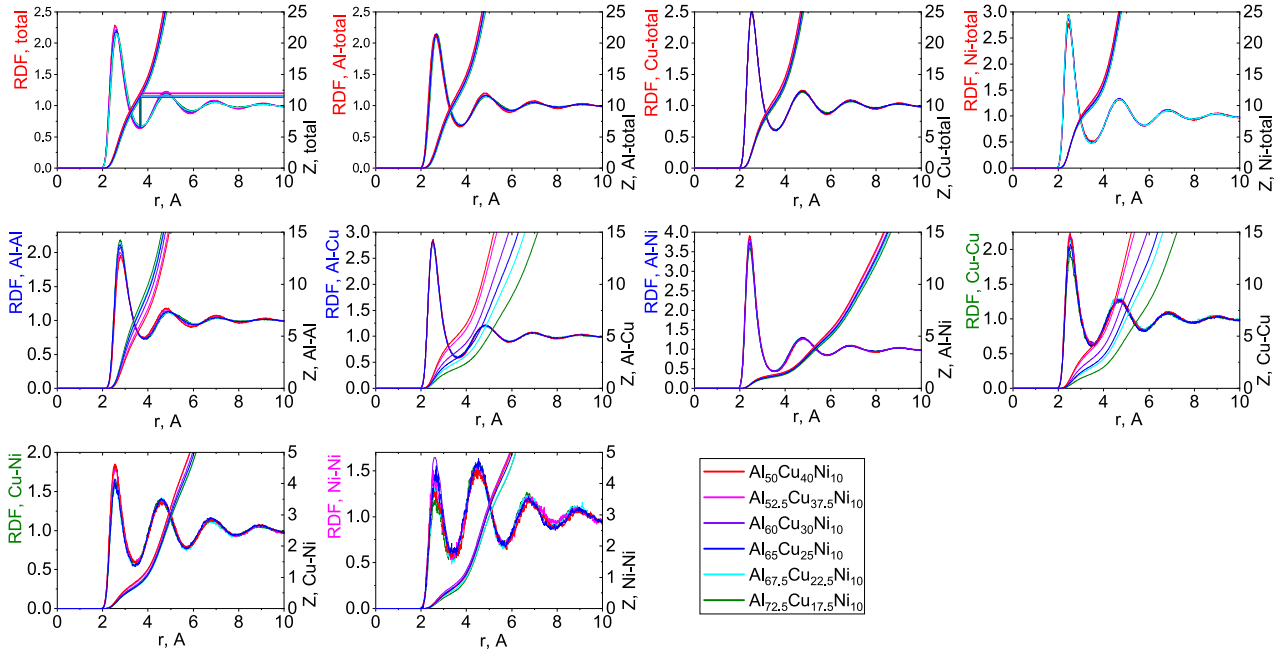

Figure 4. Total and partial RDFs $g(r)$ and coordination numbers $Z(r)$ extracted from *ab initio* molecular dynamics simulations for Al–Cu–Ni melts at 1673 K.

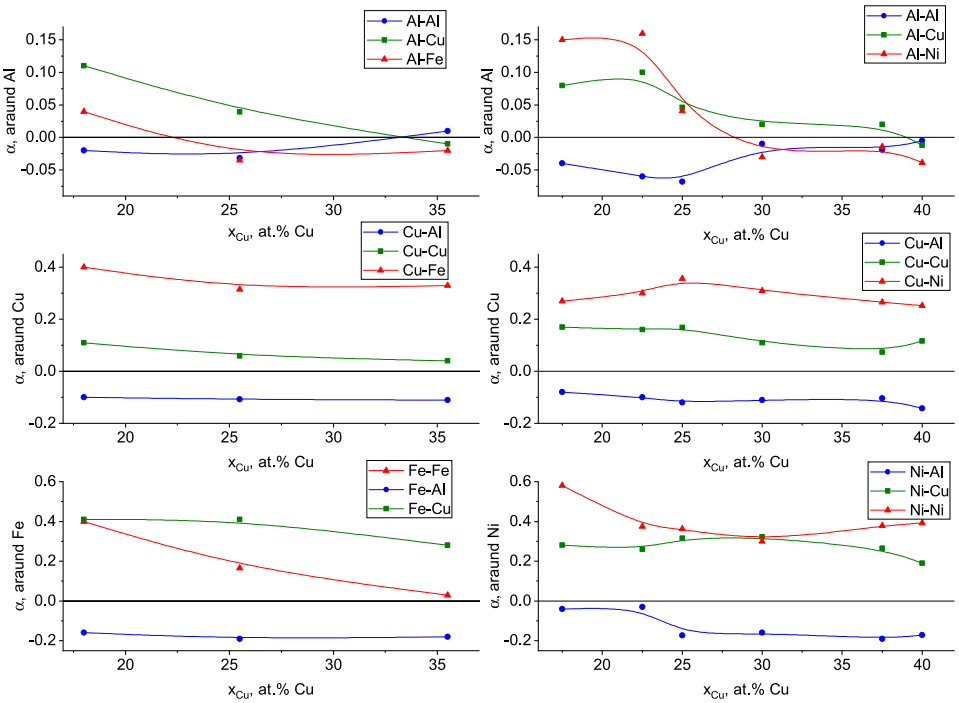

Figure 5. The concentration behavior of Warren–Cowley SRO parameters in Al–Cu–Fe and Al–Cu–Ni melts extracted from *ab initio* data. The solid lines are drawn to guide the eye.

time, $g_{\mathrm{Cu-Fe}}(r)$ and $g_{\mathrm{Fe-Fe}}(r)$ curves demonstrate different behaviour that depends on the Cu concentration, first of all, this is the ratio of the heights of the first and second peaks. For alloys with 18 and 25.5 at.% Cu, the heights of the second peaks are greater than the first, and there is an interesting effect on $g_{\mathrm{Fe-Fe}}(r)$ curves at a concentration corresponding to the i-phase (see figure 3, panel Fe–Fe): splitting the first peak of the RDF. That means the presence of two characteristic spatial scales (bond lengths) in the first coordination shell.

For the Al–Cu–Ni system, $g_{\mathrm{Ni-Al}}(r)$ also demonstrates pronounced first peak, but the values of the first minimum are not as low as for $g_{\mathrm{Fe-Al}}(r)$. The ratio of the first and second peaks $g_{\mathrm{Cu-Ni}}(r)$ and $g_{\mathrm{Ni-Ni}}(r)$ also depends on the concentration of copper. Note an essential difference between $g_{\mathrm{Cu-Fe}}(r)$

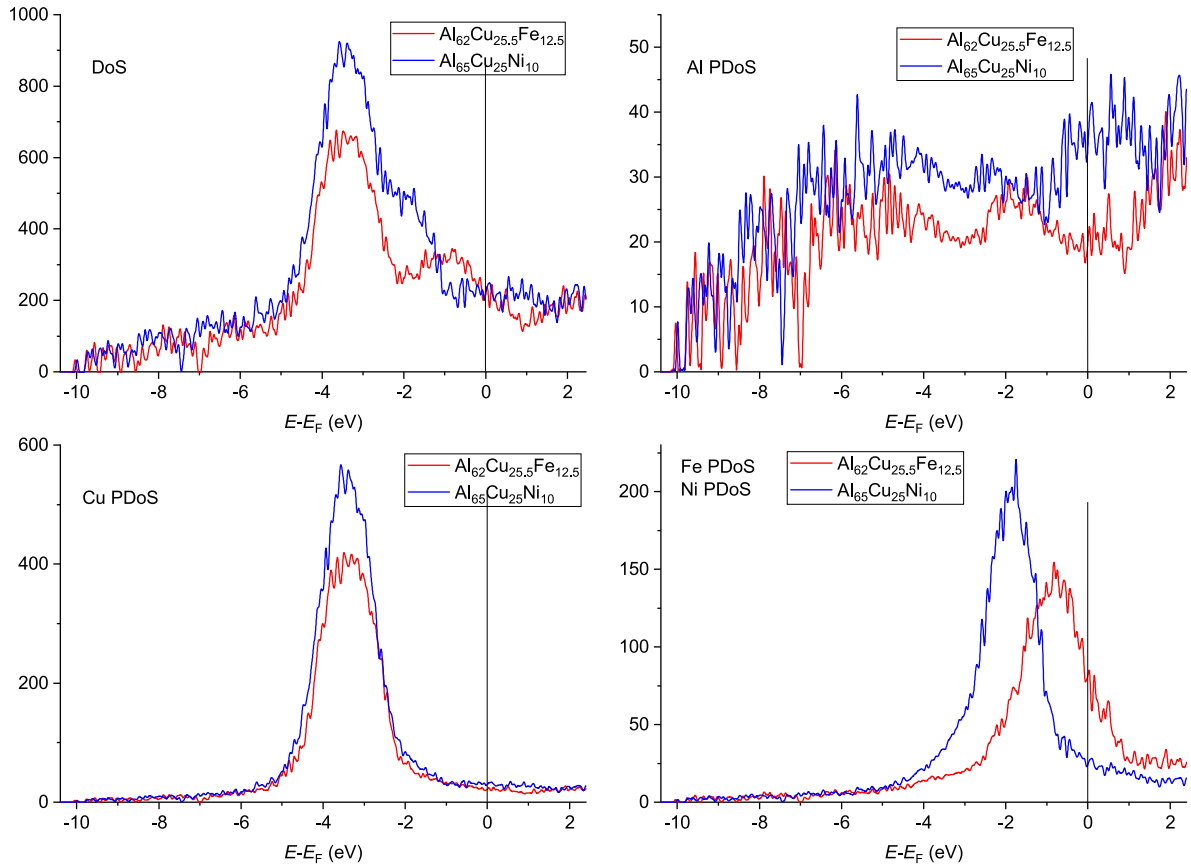

Figure 6. Total and partial densities of states for $Al_{62}Cu_{25.5}Fe_{12.5}$ and $Al_{65}Cu_{25}Ni_{10}$ melts.

and $g_{Cu-Ni}(r)$; for the former, the second RDF peak is higher than the first at low Cu concentrations. The same features are observed for $g_{Ni-Ni}(r)$ at a $x_{Cu} < 25$ at.%.

Thus, the observed features of the RDF curves in Al–Cu–(Fe,Ni) melts suggest the following general properties of effective interaction between their components: (i) Fe and Ni atoms interact strongly with Al atoms, but tend to avoid each other, especially at low x_{Cu}; (ii) Al–Fe interaction is stronger than Al–Ni; (iii) in Al–Cu–Fe alloys with $x_{Cu} < 35.5$ at.%, a pronounced separation between the Fe and Cu atoms is observed.

4. Discussion

To analyze chemical short range order (SRO) in Al–Cu–Fe and Al–Cu–Ni melts in more detail, we calculate Warren–Cowley SRO parameters α_{i-j} described in the section 2. In figure 5 we show the concentration behaviour of calculated α_{i-j} values.

As seen from figure 5, the strongest chemical interactions in Al–Cu–Fe melts are effective repulsion between Cu–Fe and Fe–Fe pairs and effective attraction between Fe–Al pairs that are in agreement with the conclusions made from the analysis of RDFs (see figures 3 and 4). At that, we see that Cu–Fe effective repulsion is almost symmetric (both α_{Cu-Fe} and α_{Fe-Cu} have high positive values at all compositions) whereas Al–Fe attraction is essentially asymmetric. Indeed, α_{Al-Fe} are close to zero and have different signs at different compositions but α_{Fe-Al} demonstrates high negative and almost concentration-independent values. This behavior suggests that strong chemical interaction between Fe and Al is reflected by the existence of Fe-centered atomic clusters with pronounced orientational ordering and chemical compositions with the excess of Al atoms.

Analysis of RDFs reveals that properties of chemical interaction in Al–Cu–Ni melts have a similar character. The strongest chemical interactions in Al–Cu–Ni melts are effective repulsion between Ni–Ni and Cu–Ni pairs and effective attraction between Ni–Al pairs at Cu concentration more than 22.5 at.%. However, Ni–Cu and Ni–Ni effective repulsions are not as pronounced as for Fe–Cu and Fe–Fe pairs.

Thus, analysis of partial RDFs and Warren–Cowley SRO parameters α_{i-j} reveals the following qualitative features of interatomic interactions in Al–Cu–Fe and Al–Cu–Ni melts: (1) relatively weak Cu–Cu and Al–Al interactions; (2) intermediate attractive interaction between Al and Cu; (3) strong attractive interaction between Al–Fe and Al–Ni (in Al–Cu–Ni systems, this interaction is manifested at $x_{Cu} > 22.5$ at.%); (4) strong Fe–Cu, Fe–Fe, and Ni–Ni effective repulsions (in the case of Fe–Fe at low x_{Cu} only). The results obtained are in close agreement with the features of the electronic structure of the studied melts. Figure 6 shows the total and partial densities of states for two alloys from each system with similar Al and Cu contents.

It can be seen from the figure 6 that the densities of electronic states at the Fermi level $n(E_F)$ of both alloys are the

same and mainly determined by s,p-states of Al, s-states of Cu and s,d-states of the transition metals (Fe, Ni). However, an analysis of partial densities of states shows that, in the Al–Cu–Ni system, the main contribution to $n(E_F)$ is determined by the s,p-states of Al. In the Al–Cu–Fe system, it is composed of s,p-states of Al and s,d-states of Fe. In Al–Cu–Ni alloy, d-electrons of Ni are mainly localized below E_F (from -4.5 to -0.8 eV); only small amounts of them reach E_F. The density of d-states of Fe is essentially higher than that for Ni and, as was mentioned above, contributes noticeably to the total density of states. However, as seen from figure 6, the half-width of the peak of Fe d-states is higher than that for Ni ($\approx$30%). That means d-states of Fe are more delocalized due to their higher hybridization (i.e. the interaction of Fe with Cu and Al). Since d-states of Fe are close to s,p-states of Al, we conclude that Fe–Al interaction is higher than Fe–Cu and Ni–Al. Thus, the features of interatomic interactions extracted from structural analysis are determined by the electronic structure of the melts.

These features are in good agreement with experimental results obtained for Al–Cu–Fe alloys as well as for similar quasicrystal-forming system, Al–Fe–Co. First, the features of interatomic interactions listed above are in qualitative agreement with phase diagrams of corresponding binary alloys. Indeed, Al–Cu and Al–Fe diagrams contain several intermetallic compounds, which suggest chemical interaction between components. At the same time, Cu–Fe diagrams demonstrate no intermetallics and the existence of a metastable liquid miscibility gap, which supposes strong effective repulsion between components. Second, the same qualitative conclusions regarding effective interactions in the icosahedral quasicrystal phase were made from the analysis of vibrational spectra [43, 44] and EXAFS spectra [45]. That means there is a correlation between the structure of the system in liquid and solid phases. Third, similar behavior has been observed experimentally in Al–Fe–Co liquids [46]. Analyzing Faber-Ziman Al–Al, TM–Al and TM–TM partial pair distribution functions (where TM = Co, Fe) the authors also observed strong chemical interaction between Al–TM and effective TM–TM first-neighbors repulsion. However, the revealed interaction features depend on the Cu concentration in the melts. The replacement of Al with Cu enhances the chemical interaction in Al–Fe and Al–Ni pairs. Indeed, the sign of the corresponding α_{i-j} (figure 5) changes in both systems at concentrations corresponding to the invariant phase transformations. Also, an increase in copper concentration leads to a weakening of the effective repulsion between Fe–Cu, Fe–Fe, and Ni–Ni (see the corresponding partial RDFs in figures 3 and 4).

In addition to the structural factors, radial distribution functions, coordination numbers and density of states, analysis of Voronoi polyhedra might give more useful information on the structure of liquids. We have performed Voronoi analysis and found very broad distributions of Voronoi polyhedra with the abundance of each polyhedron which does not exceed 2.5 at.% The most abundant polyhedra correspond to disturbed hcp/fcc and Kasper polyhedra (such as polyhedra whose $\langle n_4, n_5, n_6\rangle$ Voronoi indexes are $\langle 3,6,4\rangle$, $\langle 3,6,3\rangle$, $\langle 3,6,5\rangle$, $\langle 2,8,4\rangle$, etc). Such behavior is because the structure of the melts at elevated temperatures is highly disturbed by thermal fluctuations and so does not have any pronounced structural motifs. Investigation of the structure of supercooled liquids is needed in such a situation.

5. Conclusions

We show that the concentration dependencies of the viscosity of Al–Cu–(Fe,Ni) melts reproduce qualitatively the liquidus line. Indeed, a minimum on viscosity isotherms are observed at the concentrations corresponding to invariant transformations.

Relying on the concentration dependencies of the viscosity, we also study the structure of Al–Cu–Fe and Al–Cu–Ni melts at temperatures slightly above the liquidus line using AIMD simulations. We show that the structural characteristics extracted from the radial distribution functions of the melts make it possible to detect structural heredity between the solid and liquid phases. In particular, analyzing these correlation functions, we show that the main features of the effective interatomic interaction in the Al–Cu–Fe and Al–Cu–Ni systems are the same for both the liquid and solid states. For example, there is a pronounced effective repulsion between Cu–Fe, Ni–Ni atoms and an attraction between Fe and Al atoms. These interaction features are associated with a change in the electronic subsystem of transition metals and depend on the copper concentration; at $x_{Cu} = 35.5$ at.% in the Al–Cu–Fe system and $x_{Cu} = 37.5$ at.% in the Al–Cu–Ni system, the effective repulsion in Cu–Fe and Ni–Ni pairs ceases to be explicit.

Acknowledgments

This work was supported by Russian Science Foundation (Grant 18-12-00438). The experimental study was performed using equipment of the Shared Use Centre of Physical and Physicochemical Methods of Analysis and Study of the Properties and Surface Characteristics of Nanostructures, Materials, and Products, UdmFRC UB RAS. We thank 'Uran' supercomputer of IMM UB RAS for access. Model simulations have been carried out using computing resources of the federal collective usage center Complex for Simulation and Data Processing for Mega-science Facilities at NRC 'Kurchatov Institute', http://ckp.nrcki.ru/.

ORCID iDs

L V Kamaeva https://orcid.org/0000-0002-9141-3120
R E Ryltsev https://orcid.org/0000-0003-1746-8200
N M Chtchelkatchev https://orcid.org/0000-0002-7242-1483

References

[1] Wu Z W, Li F X, Huo C W, Li M Z, Wang W H and Liu K X 2016 *Sci. Rep.* **6** 35967
[2] Bendert J C, Gangopadhyay A K, Mauro N A and Kelton K F 2012 *Phys. Rev. Lett.* **109** 185901

[3] Ryltsev R, Klumov B and Chtchelkatchev N 2015 *Soft Matter* **11** 6991–8
[4] Ryltsev R and Chtchelkatchev N 2017 *Soft Matter* **13** 5076–82
[5] Dubinin N 2019 *J. Alloys Compd.* **803** 1100–4
[6] Bendert J and Kelton K 2013 *J. Non-Cryst. Solids* **376** 205–8
[7] Kelton K F 2016 *J. Phys.: Condens. Matter* **29** 023002
[8] Su Y, Wang X D, Yu Q, Cao Q P, Ruett U, Zhang D X and Jiang J Z 2017 *J. Phys.: Condens. Matter* **30** 015402
[9] Wang J, Li X, Pan S and Qin J 2017 *Comput. Mater. Sci.* **129** 115–22
[10] Debela T T and Abbas H G 2018 *J. Non-Cryst. Solids* **499** 173–82
[11] Tsai A P 2008 *Sci. Technol. Adv. Mater.* **9** 013008
[12] Huttunen-Saarivirta E 2004 *J. Alloys Compd.* **363** 154–78
[13] Raghavan V 2005 *J. Phase Equilib. Diffus.* **26** 59–64
[14] Prince A and Kumar K H 2005 Al–Cu–Ni (Aluminium–Copper–Nickel) *Light Metal Systems. Part 2* ed G Effenberg and S Ilyenko (Berlin: Springer)
[15] Sterkhova I and Kamaeva L 2014 *J. Non-Cryst. Solids* **401** 241–4
[16] Kamaeva L V, Sterkhova I V and Lady'anov V I 2012 *Inorg. Mater.* **48** 318–24
[17] Schick M, Brillo J, Egry I and Hallstedt B 2012 *J. Mater. Sci.* **47** 8145–52
[18] Brillo J, Chathoth S M, Koza M M and Meyer A 2008 *Appl. Phys. Lett.* **93** 121905
[19] Konstantinova N, Kurochkin A and Popel P 2011 *EPJ Web Conf.* **15** 01024
[20] Khusnutdinoff R M, Mokshin A V, Menshikova S G, Beltyukov A L and Lady'anov V I 2016 *J. Exp. Theor. Phys.* **122** 859–68
[21] Kehr M, Schick M, Hoyer W and Egry I 2008 *High Temp.—High Press.* **37** 361–9
[22] Chen W, Zhang L, Du Y and Huang B 2014 *Phil. Mag.* **94** 1552–77
[23] Pasturel A and Jakse N 2015 *J. Non-Cryst. Solids* **425** 176–82
[24] Jakse N and Pasturel A 2016 *Phys. Rev.* B **94** 224201
[25] Bel'tyukov A, Menshikova S and Lady'anov V 2015 *J. Non-Cryst. Solids* **410** 1–6
[26] Qin H O, Geng H R and Li Z Y 2011 *Appl. Mech. Mater.* **55** 913–7
[27] Kamaeva L V, Korepanov A Y and Lady'anov V I 2018 *High Temp.* **56** 514–8
[28] Bel'tyukov A, Olyanina N and Lady'anov V 2019 *J. Mol. Liq.* **281** 204–15
[29] Bel'tyukov A L and Lady'anov V I 2008 *Instrum. Exp. Tech.* **51** 304–10
[30] Olyanina N V, Bel'tyukov A L and Lady'anov V I 2015 *AIP Conf. Proc.* **1673** 020015
[31] Sterkhova I and Kamaeva L 2014 *J. Non-Cryst. Solids* **401** 250–3
[32] Kresse G and Furthmuller J 1996 *Comput. Mater. Sci.* **6** 15–50
[33] Perdew J P, Chevary J A, Vosko S H, Jackson K A, Pederson M R, Singh D J and Fiolhais C 1992 *Phys. Rev.* B **46** 6671–87
[34] Perdew J P and Wang Y 1992 *Phys. Rev.* B **45** 13244–9
[35] Kresse G and Joubert D 1999 *Phys. Rev.* B **59** 1758–75
[36] Oganov A R and Glass C W 2006 *J. Chem. Phys.* **124** 244704
[37] Oganov A R, Lyakhov A O and Valle M 2011 *Acc. Chem. Res.* **44** 227–37
[38] Lyakhov A O, Oganov A R, Stokes H T and Zhu Q 2013 *Comput. Phys. Commun.* **184** 1172–82
[39] Oganov A R and Valle M 2009 *J. Chem. Phys.* **130** 104504
[40] Humphrey W, Dalke A and Schulten K 1996 *J. Mol. Graph.* **14** 33–8
[41] Petkov V 1989 *J. Appl. Crystallogr.* **22** 387–9
[42] Warren B E, Averbach B L and Roberts B W 1951 *J. Appl. Phys.* **22** 1493–6
[43] Brand R, Coddens G, Chumakov A, Dianoux A J and Calvayrac Y 2000 *Mater. Sci. Eng.* A **294–6** 662–5
[44] Brand R, Voss J and Calvayrac Y 2001 *J. Non-Cryst. Solids* **287** 210–5
[45] Gomilšek J P, Arčon I, Kodre A and Dolinšek J 2002 *Solid State Commun.* **123** 527–30
[46] Schenk T, Simonet V, Holland-Moritz D, Bellissent R, Hansen T, Convert P and Herlach D M 2004 *Europhys. Lett.* **65** 34–40